Cell Tissue Res (2015) 362:513–527
DOI 10.1007/s00441-015-2225-5

REGULAR ARTICLE

# Molecular organization and fine structure of the human tectorial membrane: is it replenished?

**Hisamitsu Hayashi**[1,2] · **Annelies Schrott-Fischer**[3] · **Rudolf Glueckert**[3] · **Wei Liu**[4] · **Willi Salvenmoser**[5] · **Peter Santi**[6] · **Helge Rask-Andersen**[1]

Received: 24 January 2015 / Accepted: 22 May 2015 / Published online: 18 June 2015


**Abstract** Auditory sensitivity and frequency resolution depend on the physical properties of the basilar membrane in combination with outer hair cell-based amplification in the cochlea. The physiological role of the tectorial membrane (TM) in hair cell transduction has been controversial for decades. New insights into the TM structure and function have been gained from studies of targeted gene disruption. Several missense mutations in genes regulating the human TM structure have been described with phenotypic expressions. Here, we portray the remarkable gradient structure and molecular organization of the human TM. Ultrastructural analysis and confocal immunohistochemistry were performed in freshly fixed human cochleae obtained during surgery. Based on these findings and recent literature, we discuss the role of human TMs in hair cell activation. Moreover, the outcome proposes that the α-tectorin-positive amorphous layer of the human TM is replenished and partly undergoes regeneration during life.

**Keywords** Tectorial membrane · Human · Electron microscopy · α-tectorin

**Abbreviation**

| | |
|---|---|
| BM | Basilar membrane |
| HS | Hensen's stripe |
| IDC | Interdental cell |
| IHC | Inner hair cell |
| KM | Kimura's membrane |
| L | Limbus |
| LZ | Limbal zone |
| MaZ | Marginal zone |
| MN | Marginal net |
| MZ | Middle zone |
| OHC | Outer hair cell |
| RF | Radial fiber |
| SEM | Scanning electron microscopy |

✉ Hisamitsu Hayashi
hisamitsu.hayashi@surgsci.uu.se

✉ Rudolf Glueckert
rudolf.glueckert@i-med.ac.at

Annelies Schrott-Fischer
annelies.schrott@i-med.ac.at

Wei Liu
lwoo24@gmail.com

Willi Salvenmoser
willi.salvenmoser@uibk.ac.at

Peter Santi
psanti@umn.edu

Helge Rask-Andersen
helge.rask-andersen@akademiska.se

[1] Department of Surgical Sciences, Head and Neck Surgery, section of Otolaryngology, Uppsala University Hospital, SE-751 85 Uppsala, Sweden

[2] Department of Otolaryngology, Gifu University Graduate School of Medicine, 1-1 Yanagido, Gifu, Gifu 501-1194, Japan

[3] Department of Otolaryngology, Medical University of Innsbruck, Anichstr. 35, A-6020 Innsbruck, Austria

[4] Department of Surgical Sciences, Section of Otolaryngology, Uppsala University Hospital, SE-751 85 Uppsala, Sweden

[5] Institute of Zoology, University of Innsbruck, Innsbruck, Austria

[6] Department of Otolaryngology, University of Minnesota, Lions Research Building, 2001 Sixth St. SE, Minneapolis, MN 55455, USA

STL Subtectorial layer
TEM Transmission electron microscopy
TM Tectorial membrane

## Introduction

> "I hope that one day we can enshroud the elusive nature of the tectorial membrane and its relationship to the organ of Corti". David Lim (1986)

The tectorial membrane (TM) is an acellular matrix that spirals along the cochlea overlying the hair cells. Medially, it is firmly attached to the spiral limbus. Recent studies have shown that the TM can play a more active role in the ears' processing of sound than to just act as a stiff bar to generate shearing motions of the stereocilia bundles of hair cells. The TM may produce traveling waves in vitro and possibly contribute to the electromotor response of OHCs (Ghaffari et al. 2007; Hubbard 1993; Sellon et al. 2014). Changes in TM stiffness, radial fiber anisotropy, longitudinal coupling and graded viscoelasticity from base-to-apex seem to play crucial roles (Meaud and Grosh 2010; Richter et al. 2007; Sellon et al. 2014). Mutational changes affecting TM protein constituents result in a broad spectrum of hearing impairment ranging from mild to profound (20–110 dB HL on all frequencies) in severity (Verhoeven et al. 1998; Mustapha et al. 1999; Simmler et al. 2000; Verpy et al. 2001; Alasti et al. 2008; Zheng et al. 2011). Equally, studies on targeted gene disruption have provided new insights in the role of TM in regulating cochlear amplification and frequency tuning (Legan et al. 2000; Lukashkin et al. 2004; Russell et al. 2007; Sellon et al. 2014).

TM morphology, including its ultrastructure, has been studied thoroughly in several animal models (Hilding 1952; Lim 1972; Tanaka and Smith 1975; Steel 1983; Kimura 1966; Hoshino 1977), but there have been relatively few investigations in humans (Hoshino 1981; Kawabata and Nomura 1981; Rask-Andersen et al. 2012). Here, we describe the ultrastructure and macromolecular composition (via laser confocal immunohistochemistry) of the human TM. Human cochleae were drilled out in patients with life-threatening petro-clival meningioma after ethical permission and patient consent (M&M) were obtained. It was thereby possible to explore the fine structure of the human TM under non-pathological conditions, as the patients had normal audiograms. At dissection, the reticular lamina and the TM surfaces could be put side by side. Analysis of these structures via transmission electron microscopy (TEM), scanning electron microscopy (SEM), and confocal fluorescent immunochemical microscopy confirmed the anisotropy of the human TM from base to apex. Structural graded modifications, including the hair cell interactive surfaces may optimize deflection of the anisotropic hair bundles.

## Material and methods

The study of human materials was approved by the local ethics committee (no. 99398, 22/9 1999, cont., 2003, Dnr. 2013/190) and patient consent was obtained. The studies adhered to the Helsinki declaration.

### Fixation and sectioning of human cochlea

Histological processing of the TM after long-term EDTA-storage and surgical drilling can influence preservation and is a limiting factor of this study (Kronester-Frei 1978; Steel 1983). Care was taken to preserve scala media integrity during fixation. Eleven cochleae from adult patients (4 male, 7 female; ages 43–72 years) with normal pure-tone thresholds for their ages were dissected as whole pieces during petro-clival meningioma surgery. In the operating room, four cochleae were immediately placed in 4 % paraformaldehyde in 0.1 M phosphate buffered saline (PBS; pH 7.4). After a 24-h fixation, the fixative was replaced with 0.1 M PBS, then with a 0.1-M Na-EDTA solution at pH 7.4 for decalcification. After 4 weeks, the thoroughly decalcified cochleae were rinsed with PBS. For frozen sections, the cochleae were embedded in Tissue-Tek (OCT Polysciences), rapidly frozen and sectioned at 8–10 μm using a Leica cryostat microtome. The frozen sections were collected onto gelatin/chrome-alum-coated slides and stored below –70 °C before immunohistochemistry. The fixation and processing of perilymphatically fixed human inner ear specimens has been described earlier (Spoendlin and Schrott 1988).

### Antibody, immunohistochemistry and lectin labeling

The antibody against laminin-β2 was a monoclonal antibody from rat (catalog #05-206, Millipore; dilution 1:100). It specifically recognizes the β2 chain of laminin. The type IV collagen antibody was a goat polyclonal antibody (catalog #AB769, Millipore; dilution 1:10). It has less than 10 % cross reactivity with collagen types I, II, III, V and VI. The antibody against collagen type II was a monoclonal antibody from the mouse (catalog #CP18, Millipore; dilution 1:100). It was specific for type II collagen protein. The α-tectorin and β-tectorin antibodies were both polyclonal from goat (catalog #sc-18035, Santa Cruz; #sc-165671, Santa Cruz; dilution 1:100). The antibody data are summarized in Table 1. Immunohistochemistry procedures on cochlear sections were described in previous publications (Liu et al. 2009). Briefly, incubation of sections on slides with a solution containing the antibodies was carried out under a humid atmosphere at 4 °C for 20 h. After rinsing in PBS (3×5 min), the sections were subsequently incubated at room temperature for 2 h with a secondary antibody (conjugated to either Alexa Fluor 488 or 555; Molecular Probes). We also stained sections with the lectin soybean agglutinin (SBA; Molecular Probes; dilution 1:200) that

**Table 1** Antibodies used in the current study

| Antibody | Characteristic | Dilution | Host | Catalog number | Company |
|---|---|---|---|---|---|
| Laminin β 2 | Monoclonal | 1:100 | Rat | 05-206 | Millipore |
| Type IV collagen | Polyclonal | 1:10 | Goat | AB769 | Millipore |
| Type II collagen | Monoclonal | 1:100 | Mouse | CP18 | Millipore |
| α -tectorin | Polyclonal | 1:100 | Goat | sc 18035 | Millipore |
| β -tectorin | Polyclonal | 1:100 | Goat | sc 165671 | Millipore |

recognizes the presence of *N*-acetyl galactosamine (Rubio et al. 1994). It was added to the sections and mixed with a secondary antibody conjugated to Alexa Fluor 555 because the SBA was tagged with Alexa Fluor 488. The sections were counterstained with the nuclear stain DAPI (4',6-diamidino-2-phenylindole dihydrochloride) for 5 min, then rinsed with PBS (3×5 min). The sections were mounted with a VECTASHIELD mounting medium.

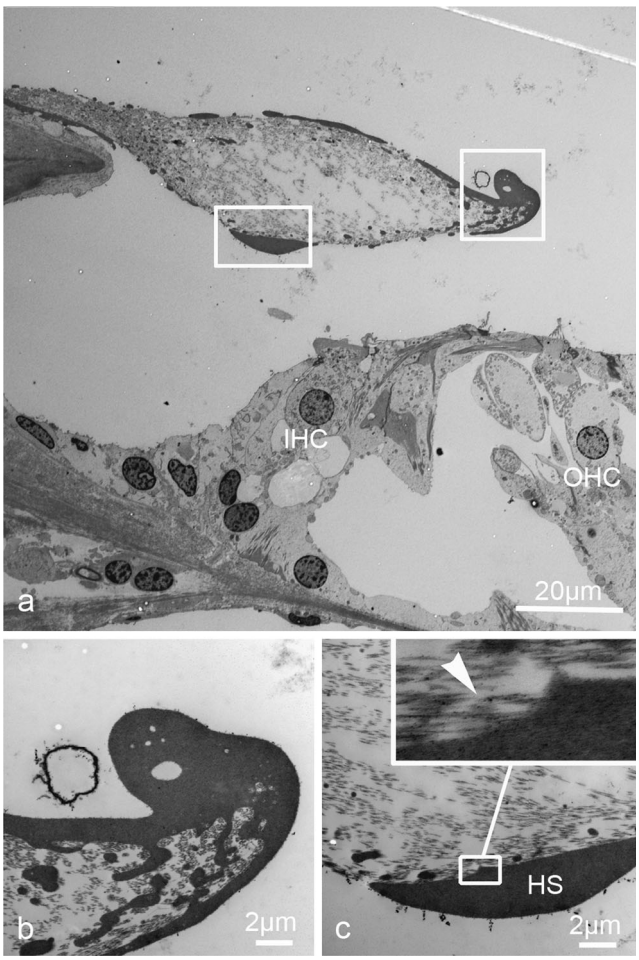


**Fig. 1** TEM of the tectorial membrane of the basal turn. **a** A low-magnification TEM image showing the TM of the basal turn. The *framed areas* are magnified in (**b**) and (**c**). *OHC* outer hair cell, *IHC* inner hair cell. 67 years old. **b** The lateral margin of the TM is electron-dense and tilted upward. **c** Hensen's stripe (*HS*) on the inferior surface of the TM is prominent. The *inset* shows that the radial collagen fibers (*arrowhead*) and homogeneous material of Hensen's stripe are coalesced

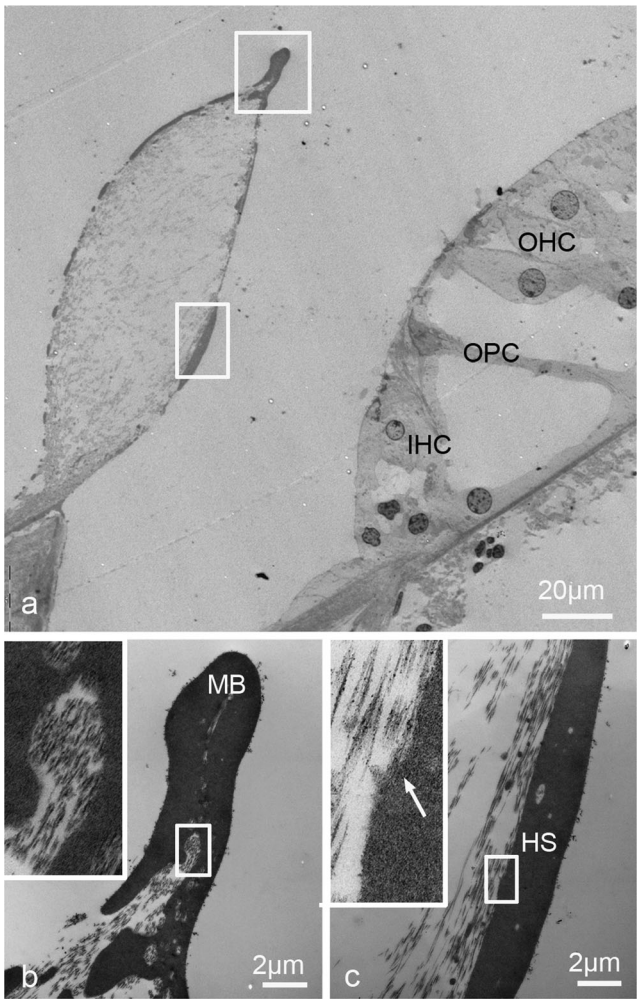


**Fig. 2** TEM of the tectorial membrane of the middle turn. **a** A low-magnification TEM image showing the TM and organ of Corti. The *framed areas* are magnified in (**b**) and (**c**). 54-year-old female. *OHC* outer hair cell, *IHC* inner hair cell, *OPC* outer pillar cell. **b** The lateral part of the TM displays a thinned-out portion of marginal band (*MB*) in which collagen fibers fuse with homogeneous material. **c** Hensen's stripe (*HS*) of the middle turn is comparatively flat. The radial collagen fibers penetrate inside the HS (see *arrow* in *inset*)

**Table 2** Width, thickness, fibril density of the TM, and thickness of the radial fiber (RF) bundles at each turn of the human cochlea

| Turn of the cochlea | Width (μm) Maz+MZ | MaZ | MZ | Thickness (μm) | Fibril density (number/μm) | Thickness of RF bundles (μm) |
|---|---|---|---|---|---|---|
| Hook | 68 | 13 | 55 | 19 | 6.0 | 1.4 |
| Lower basal | 86 | 14 | 74 | 24 | 6.6 | 1.6 |
| Upper basal | 111 | 21 | 90 | 22 | 8.2 | 0.8 |
| Lower middle | 160 | 22 | 138 | 45 | 3.5 | 0.8 |
| Upper middle | 186 | 48 | 138 | 64 | 3.5 | 0.5 |

(Thickness and fibril density were measured perpendicularly at the center of Hensen's stripe.)

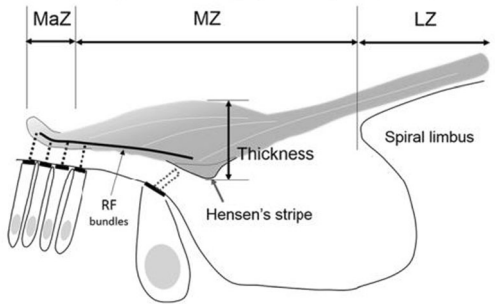


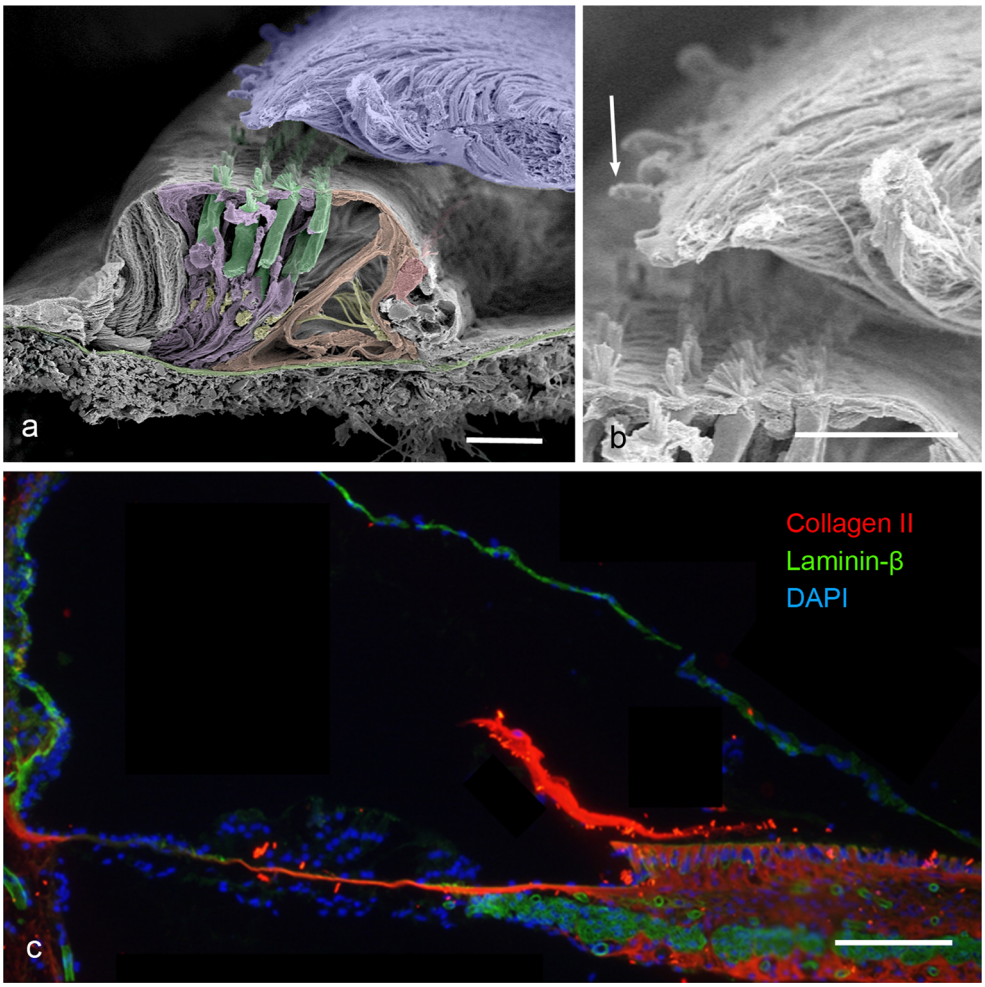


**Fig. 3** SEM and immunohistochemistry of the human tectorial membrane. **a** SEM of the organ of Corti at the upper second turn. Various cells are pseudocolored. The tectorial membrane (*blue*) contains fibers. 53-year-old female. **b** The marginal net of the tectorial membrane (*asterisk*) displays short processes (*arrow*). **c** The tectorial and basilar membranes express collagen II (*red*). 51-year-old male. *Scale bar* 50 μm

### Imaging and photography

The stained sections were investigated with an inverted fluorescence microscope (Nikon TE2000; Japan) equipped with a spot digital camera and with three filters (for emission spectra maxima at 358, 461 and 555 nm). Both the microscope and camera were connected to a computer system with image software (NIS Element BR-3.2; Nikon) installed. Relevant functions of the software included image merging and a fluorescence intensity analyzer. For laser confocal microscopy, the same microscope was used, equipped with a laser emission and detection system with three different channels. The optical scanning and image-processing tasks were run by the program Nikon EZ-C1 (v.3.80), including the reconstruction of Z-stack images into projections or 3D images.

### Transmission electron microscopy (TEM)

In the operating room, three cochleae were immediately placed in 3 % glutaraldehyde in 0.1 M PBS (pH 7.4). After a 24-h fixation, the fixative was replaced with 0.1 M PBS and a 0.1 M Na-EDTA solution at pH 7.4 for decalcification (Tylstedt et al. 1997). To further improve fixation and ultrastructural preservation, one cochlea was fixed in 2 % glutaraldehyde in an oxygenated fluorocarbon blood-substitute vehicle (Møller et al. 2013; fixative provided by Klaus Qvortrup, Copenhagen Department of Anatomy). Human specimens were analyzed at inner ear research laboratories in Uppsala and Innsbruck. Tissue was rinsed in cacodylate buffer, followed by fixation with 1 % osmium tetroxide at 4 °C for 4 h. Subsequently, the cochleae were decalcified in 0.1 M Na-EDTA, pH 7.4, for 6 weeks. After decalcification, a midmodiolar section was generated and the two halves were dehydrated in increasing concentrations of ethanol and acetone prior to incubation in a liquid epoxy resin diluted with acetone at a ratio of 30–70 % for 3 h. The specimens were infiltrated with a mixture of Epon and acetone in equal proportions at 4 °C overnight in closed vials. The next day, a mixture of 70 % epoxy resin and 30 % acetone replaced the liquid for 3 h. Subsequently, tissue samples were incubated twice in 100 % Epon at 4 °C, first for 3 h, and then overnight. The next day, the pure epoxy resin was changed and the specimens were infiltrated with Epon in a vacuum chamber for 4 h. Sections with a thickness of 1 μm were cut on a Leica UC6 microtome, lightly stained with toluidine blue at 60 °C and then examined by using a light microscope. For TEM analysis, specimens were then trimmed and ultrathin sections (90 nm thickness) were acquired and transferred to pioloform F (polyvinylacetate)-coated slot grids. Staining was performed within an automated system (Leica EM Stain) with uranyl acetate (5 g/l for 30 min) and lead citrate (5 g/l for 50 min) at 25 °C. The various turns of the cochlea were analyzed and the tectorial membranes from the lower basal, upper basal, lower middle, and upper middle regions were sectioned separately. Sections were viewed in a JEOL 100 SX electron microscope (Uppsala), and in Zeiss LIBRA (Institute of Zoology, Innsbruck) and Philips CM 120 (Division of Anatomy, Histology and Embryology, Innsbruck) transmission electron microscopes.

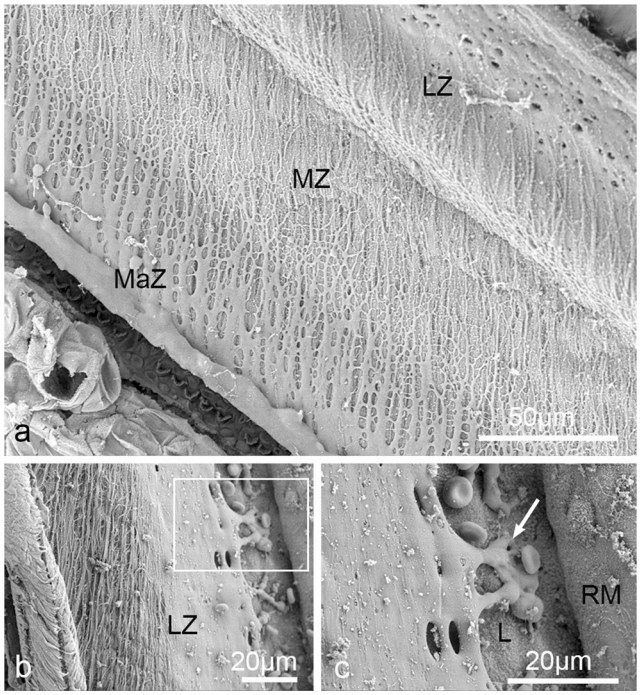


**Fig. 4** SEM of the superior surface of the human tectorial membrane. **a** The surface shows fibrous striations directed apically. 54-year-old female. **b** Medially, the LZ has a smooth surface. The *framed area* is magnified in (**c**). **c** At a higher magnification, this surface material can be seen to be closely associated with the surface layer of the interdental cells (*arrows*). *MaZ* marginal zone, *MZ* middle layer, *LZD* limbus zone, *RM* Reissner's membrane, *L* Limbus

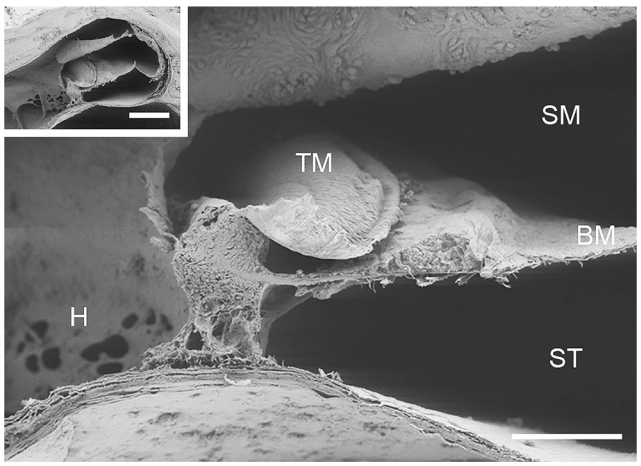


**Fig. 5** SEM of the tectorial membrane at the helicotrema. The inset in Fig 3 shows the entire apex of the cochlea. 54-year-old female. *SM* scala media, *ST* scala tympani, *TM* tectorial membrane, *BM* basilar membrane, *H* helicotrema. *Scale bar* 100 μm

### Scanning electron microscopy (SEM)

Three cochleae were fixed in 3 % glutaraldehyde in phosphate-buffered saline (PBS), pH 7.4; dehydrated in graded ethanol (70, 80, 90, 95, and 100 %; 10 min each); critical point-dried; and attached to aluminum stubs (Rask-Andersen et al. 2012). The specimens were coated in a BALTECH MED020 Coating System with gold–palladium to a nominal depth of 10–12 nm and viewed in a ZEISS DSM982 Gemini field emission electron microscope operating at 5 kV. The maximal resolution at this voltage was estimated to be approx. 2 nm. Digital photos were taken at 1280–1024 ppi resolution. Measurements were performed using the image analysis software Image Pro 4.5.1.29 (Media Cybernetics).

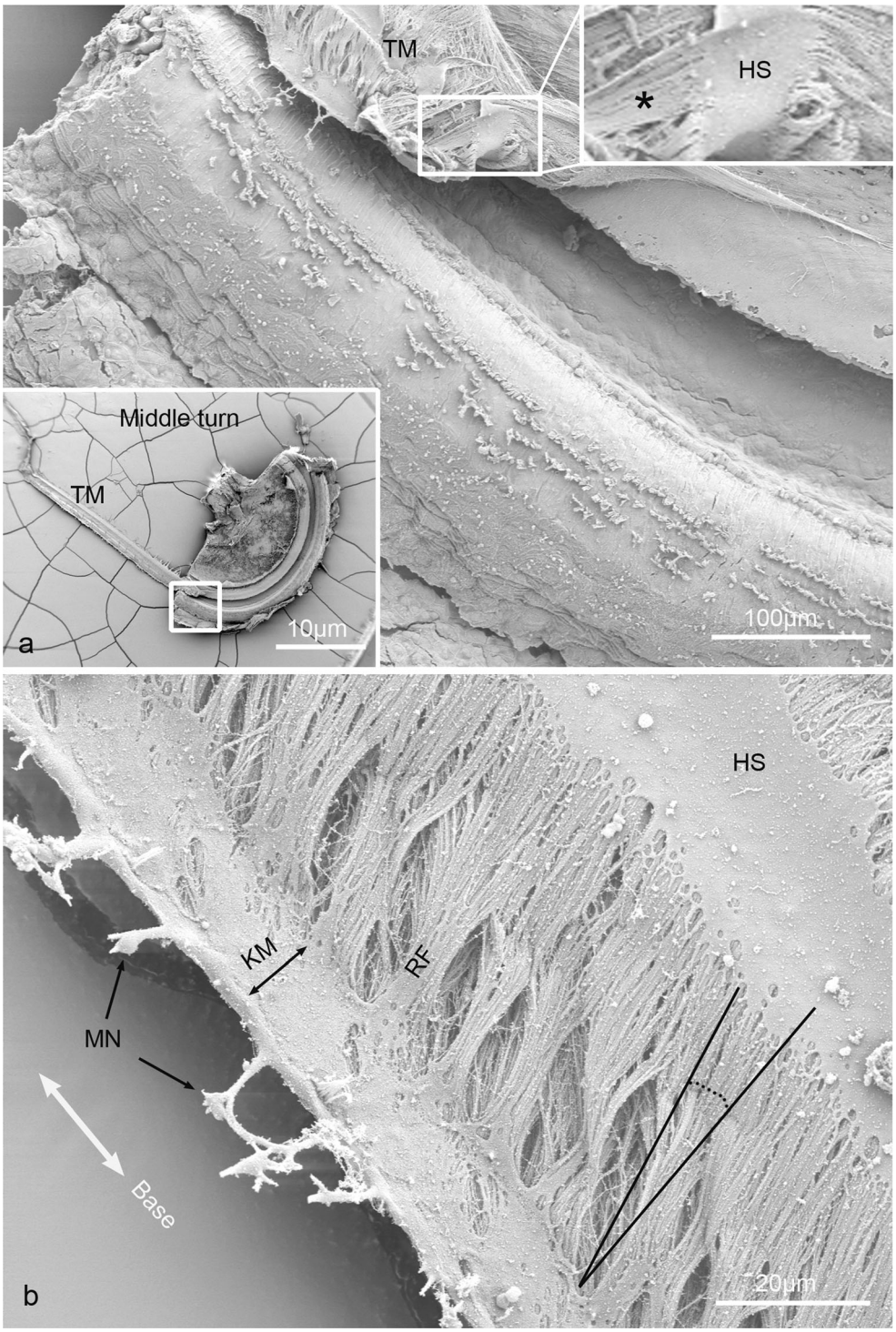


**Fig. 6** SEM of the inferior surface of the human tectorial membrane. **a** The tectorial membrane was "stripped" away from the acoustic crest and placed with its inferior surface facing upwards (*left inset*). The *framed area* is magnified (middle turn). The *right inset* shows Hensen's stripe with radial fibers (*asterisk*) running from the marginal net. *HS* Hensen's stripe, *TM* tectorial membrane. 55-year-old male. **b** Radial fiber (*RF*) bundles run along the inferior surface and merge with the HS and Kimura's membrane (*KM*). *MN* marginal net

### Tectorial membrane dimensions

The radial widths and thicknesses of the TM in sections at various turns were assessed from TEM. The thickness was measured from the superior surface of the TM to the inferior surface at the center of Hensen's stripe. The diameter of the radial fiber bundles running inferiorly from the marginal band to Hensen's stripe was measured from TEM of radial sections. Fibril density indicated the number of fibrils intersecting a line on which the thickness of the TM was measured. In one completely preserved hemi-sectioned cochlea we assessed, via SEM (on the mid-modiolar profile), the length of the longest stereocilia of the OHCs and IHCs at five different levels (lower basal, upper basal, lower middle, upper middle and apical turn).

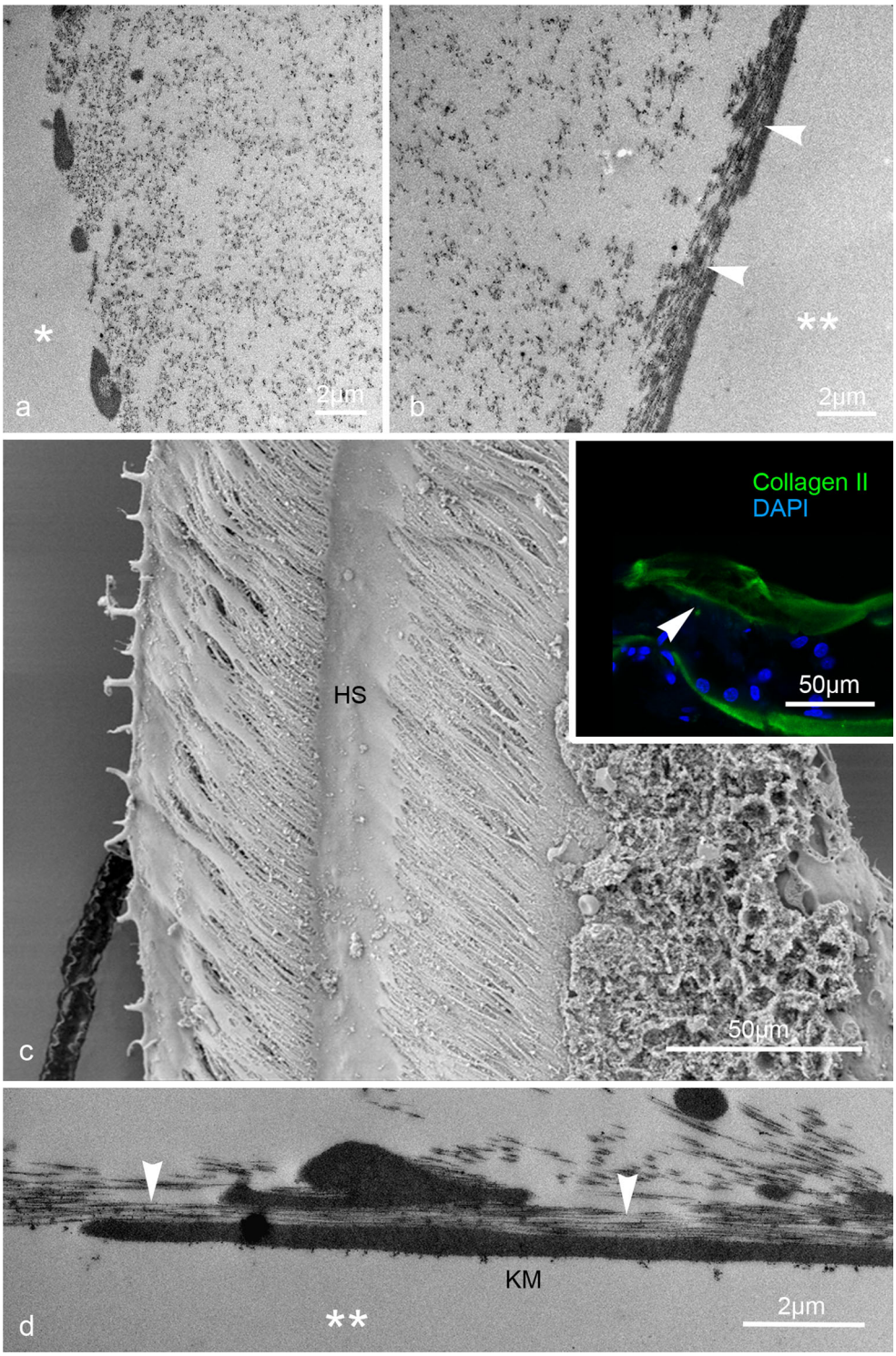


**Fig. 7** TEM, SEM and immunohistochemistry of the radial fiber bundles of the human tectorial membrane. **a**, **b** TEM shows a band of radial fibers (*arrowheads*) associated with the subtectorial surface (*double asterisk*) but not at the supratectorial surface (*asterisk*). 54 year-old female. **c** SEM showing the inferior surface of the human tectorial membrane; *inset* the collagen II immunopositive fibers (*green*, *arrowheads*) which are more prominent inferiorly. *HS* Hensen's stripe. **d** These fibers (*arrowheads*) can be seen to be closely related with Kimura's membrane (*KM*). *Double asterisk* indicates subtectorial space. 57-year-old male

## Results

The TM is generally described as consisting of three different parts (Lim 1986); the limbal zone (LZ), the middle zone (MZ) and the marginal zone (MaZ). This organization was also demonstrated in the human TM.

### General anatomy

The TM showed considerable anisotropy along the cochlear spiral. The TM size increased from base to apex. The LZ overlying the spiral limbus had a medial part that was smooth-surfaced, while the larger lateral part was covered by a net. TEM of radial sections showed that only the lateral part contained fibrous elements and represented the LZ, while the medial part contained an amorphous substance beneath the LZ. The MZs overlaid the inner sulcus and IHCs, while the MaZ superimposed the OHC region (Figs. 1 and 2). The width of the MZ and MaZ increased from 68 μm at the "hook" region to 186 μm at the upper middle turn (Table 2). The thickness of the TM measured at the level of Hensen's stripe increased from 19 μm at the "hook" to 64 μm at the upper middle turn. The TM contained a meshwork of thin fibrils, which was particularly notable in SEM images (Fig. 3a, b). Immunohistochemistry revealed that the TM expressed collagen II (Fig. 3c). In the TEM image, the fibril density in the central core of the TM decreased from the base to the apex (6.0–3.5 fibers/μm).

### Superior surface and covering net of the TM

The superior surface of the TM was covered in a radial net that also shaped the marginal band (Fig. 4). The covering net was slanted in the apical direction, approximately 45° relative to the MZ (Fig. 4). A SEM image of the supero-medial surface of the human TM revealed that it was smooth with circular perforations. The covering net lay from the apical surface of the interdental cells (IDC) laterally (Fig 4b, c). At the helicotrema, the TM terminated in a rounded end overlying the thinnest and most apical part of the organ of Corti (Fig. 5).

### Inferior surface - marginal net (MN), Hensen's stripe (HS) and Kimura's membrane (KM)

A SEM image of the inferior surface in the middle turn is shown in Figs. 6, 7 and 8. The TM was "stripped off" from the acoustic crest and placed with its inferior surface facing upwards. The prominent features are Hensen's stripe and the marginal band consisting of a marginal net and Kimura's membrane. The surface displayed radial fiber bundles running between Hensen's stripe and the marginal band. At places, the surface was covered with smooth-surfaced material. On the basal side, the bundles were more densely packed and thicker (Table 2). The fibers were slanted in an apical direction. SEM revealed the physical relationship between the fiber strings and Hensen's stripe (Fig. 6a). TEM and immunohistochemistry provided support that radial collagen II fibers were more prominent at the inferior aspect of the MZ (Fig. 7).

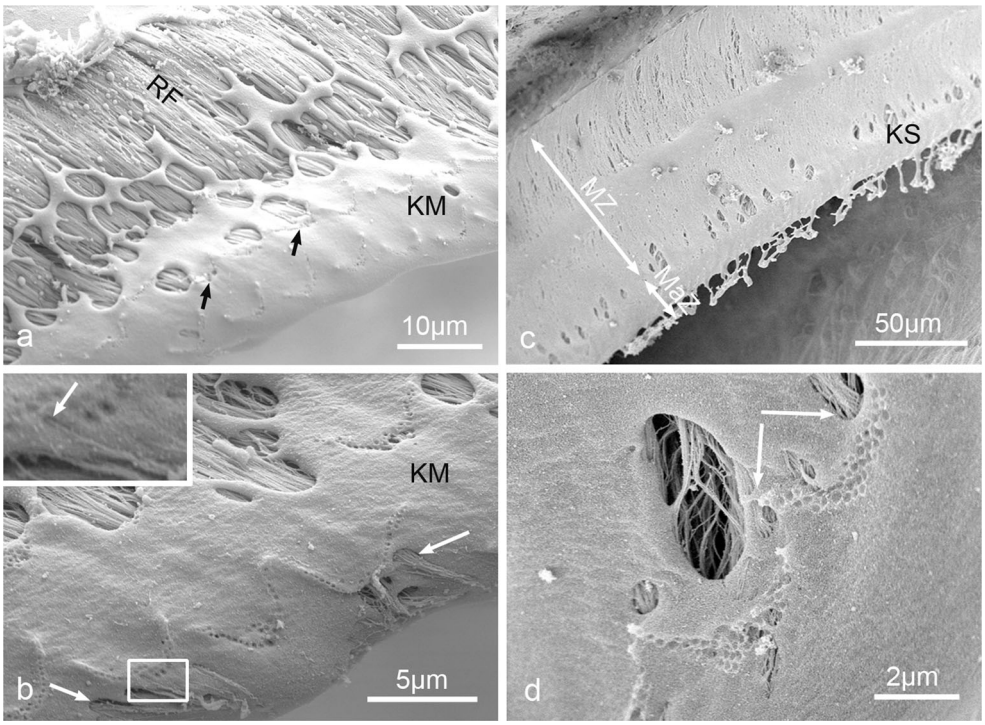


**Fig. 8** SEM of the inferior surfaces of the TM from the basal turn (**a**, **b**) and the middle turn (**c**, **d**). **a** The marginal band forms a plate (Kimura's membrane, *KM*) in which several imprints by the three rows of OHCs can be seen. There is no marginal net. The second row's imprint (*arrows*) is partially preserved. The radial fibers (*RF*) continue to the rim of the marginal band. 55-year-old male. **b** Some fibers (*arrows*) can be seen in close relation to the imprint, appearing to emerge through it (*inset*). **c** The junction between the MZ and MaZ with the first row of OHC imprints. 52-year-old male. **d** An RF reaches directly beneath the imprint (*arrows*)

An MN consisted of distal struts overlying the fourth row of OHC stereocilia (Figs. 3b, 8a, 9a, b). An MN was seen in the upper basal, middle and apical turns. Basally and at the hook, an MN was not observed. Instead, a marginal band with a smooth, curved rim that curled superiorly was present (Figs. 1, 2). The marginal band formed an inferior plate (Kimura's membrane), with imprints from 3-4 stereocilia rows of the OHCs (Figs. 8, 9). The radial fibers were closely related to the imprints (Fig. 8b, d).

Hensen's stripe varied in structure along the cochlea. It was smooth and protruded into the subtectorial space, but could be shallow. The width ranged from 17 μm at the base to 28 μm at the upper middle turn (Figs. 1 and 2). IHC stereocilia made no imprints in Hensen's stripe. The longest IHC stereocilia varied in length from approximately 1–3 μm in the "hook" and lower basal turn to approximately 7 μm at the apex (Table 3, Fig. 10). Their width was 280–300 nm at their mid-portion. The distal tips were sometimes wider and flat. IHC stereocilia narrowed into a rootlet at the base which was anchored in the cell body. The short IHC stereocilia were thin, having about one third of the width of the long stereocilia. There were no recognizable interciliary links. IHC stereocilia of the same row often showed different lengths. The number of stereocilia was approximately 40–60 per cell. A remnant kinocilium was often observed laterally (Fig. 10a, b). There were three to four fairly linear rows of OHC stereocilia, with the longest positioned laterally. The OHCs stereocilia tips were sometimes capped with adhesive extracellular material from the TM (Fig. 9d).

**Table 3** The length of the longest stereocilia of the hair cells in each turn of human cochlea

| Stereocilia length (μm) | | | |
|---|---|---|---|
| | IHC | OHC | |
| Basal turn | 3.6 | 3.5 | (3rd row) |
| Lower middle | 6.9 | 6.1 | (3rd row) |
| Upper middle | 7.1 | 5.2 | (1st row) |
| Apical turn 1 | 5.1 | 5.2 | (1st row) |
| Apical turn 2 | 7.5 | 6.9 | (3rd row) |

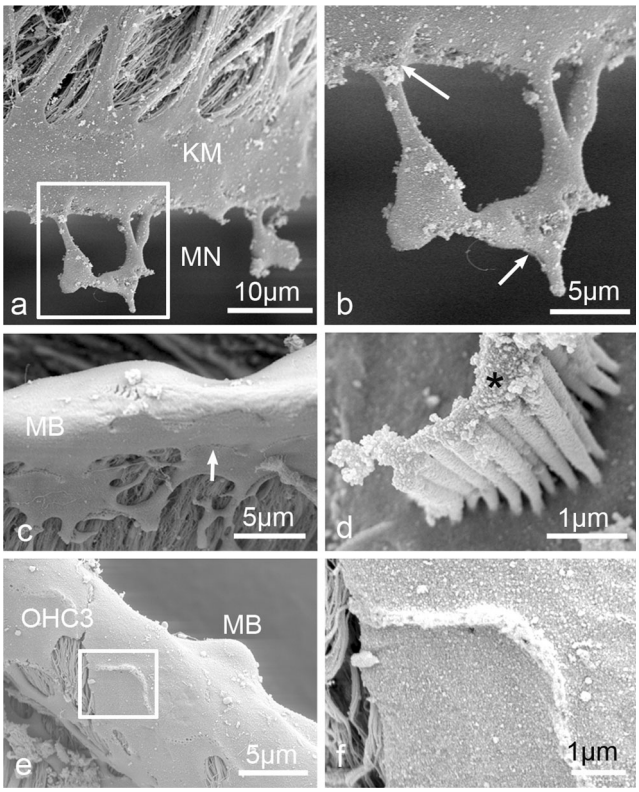


**Fig. 9** SEM of human tectorial membrane at low and high frequency regions of the cochlea. **a** The inferior surface of the TM at upper second turn of the cochlea. A smooth distal plate (Kimura's membrane, *KM*) contains several marginal struts that form a marginal net (*MN*). The *framed area* is magnified in (**b**). 52-year-old male. **b** OHC stereocilia imprints (*arrows*) from the various rows can be seen on the MN. **c** The inferior surface of the TM at the basal turn of the cochlea. A blunted marginal band (*MB*) is seen. *Arrow* indicates OHC stereocilia imprints on the inferior surface. **d** OHC stereocilia from the basal turn contain TM material (*asterisk*). 54-year-old female. **e**, **f** TM from the "hook" region of the cochlea. Modified OHC imprints can be seen possibly representing area of absent hair cells. *OHC3* Imprints from outer hair cell row 3. The framed area is magnified in (**f**). 54-year-old female

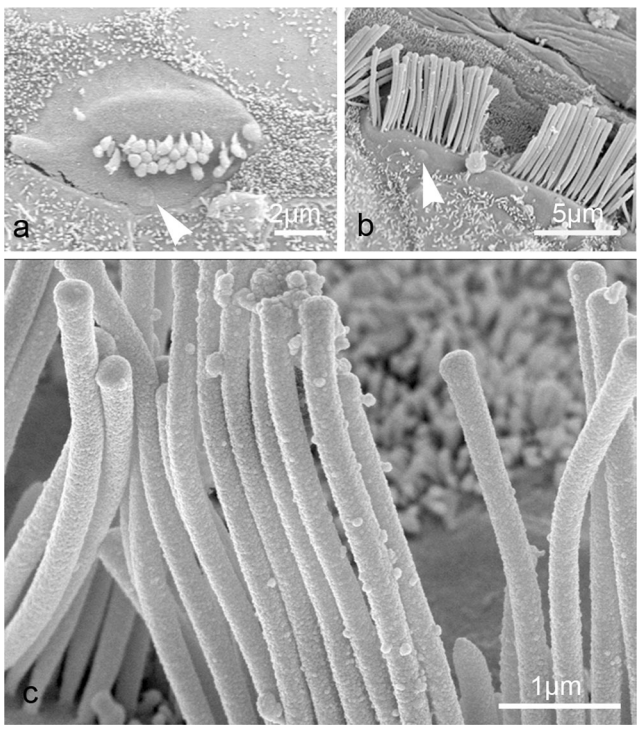


**Fig. 10** SEM of IHC stereocilia in the human cochlea. **a** IHC stereocilia in the "hook" region have a length of 1 μm at most. *Arrowheads* indicate the remnant of kinocilium. 55-year-old male. **b** IHC stereocilia of the middle turn have a longer length than those in the hook region. **c** IHC stereocilia at the apex have no apparent attached material on the tips but instead smooth surfaces

### Expression pattern of α-tectorin

The radial fibers of the TM were found to express collagen II. The TM also expressed α-tectorin, the expression of which was strongest at the borders of the TM and continued peripherally into the marginal zone border, Hensen's stripe and MZ (Fig. 11d). The expression was also spotty and seemed to correspond to the focal electron-dense material observed with TEM. The central region of the TM expressed punctate regions of α-tectorin-immunoreactivity via confocal microscopy. The LZ expressed collagen II and punctate areas of α-tectorin (Fig. 11). α-Tectorin was also strongly expressed in the subtectorial space beneath the LZ (Fig. 11a, d) as well as in the IDCs. With TEM, this layer represented the electron-dense layer (Fig. 11b). The surface material of the inner sulcus cells also expressed α-tectorin and displayed a similar electron-dense material via TEM (Fig. 11b, c). α-Tectorin staining was seen strongly in the outer circumference of the TM in the high frequency region, but seemed weaker and more scattered in the low frequency region. Lectin staining showed a somewhat similar tendency, being more positive from apex to base. No β-tectorin immunoreactivity could be verified.

### Limbal zone and interdental cells

SEM images of cochlea show the spiral limbus and pyramids of the dental processes (Fig. 12a, b). The processes expressed collagen IV (Fig. 12c, d). The IDCs are found amid these protrusions and are bordered by a continuous basement membrane expressing laminin-β2 and collagen IV. A number of IDCs form conglomerates surrounded by a common basement membrane. The IDCs contained rich amounts of electron-dense vesicles. Occasionally, the space between conglomerate cells contained electron-dense vesicles. The cell architecture and IDC configuration varied greatly in the spiral limbus along the cochlear spiral.

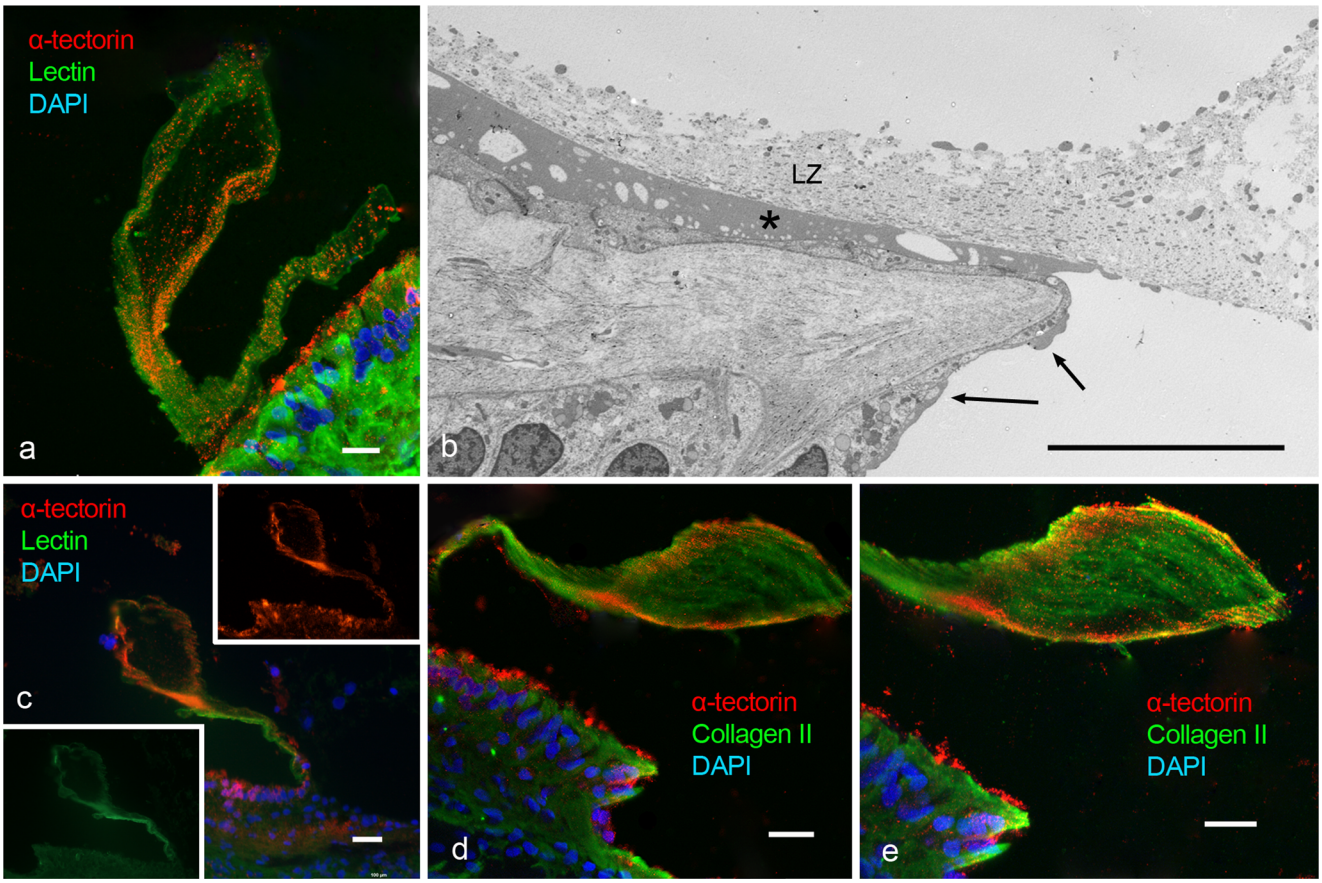


**Fig. 11** TEM and immunohistochemistry of the human tectorial membrane. **a** A confocal micrograph of the main body and LZ. The LZ and a marginal zone of the TM are lectin-positive (*green*). There is also an expression of α-tectorin (red). Lectin staining is negative in the core of the TM body. The surface layer of the interdental cells shows a strong expression of α-tectorin. 52 year-old female. **b** TEM of the LZ. An electron-dense glycoprotein material (*asterisk*) is seen on the surface of the inner sulcus cells (*arrows*). It appears as small electron-dense dots in the TM. This image was obtained following oxygenated fluorocarbon and 2 % glutaraldehyde fixation. 54-year-old female. **c** The expression of α-tectorin in the TM. α-Tectorin (*red*) is also expressed in the interdental cells and inner sulcus cells. 52 year-old female. **d** Confocal microscopy of the human TM shows the expression of collagen II in the MaZ and MZ. α-Tectorin expression is strong in the border, and there is some expression in the center of the TM. The surface of the interdental cell layer expresses α-tectorin. **e** Same as (**d**) with rendered images. *Scale bar* 20 μm

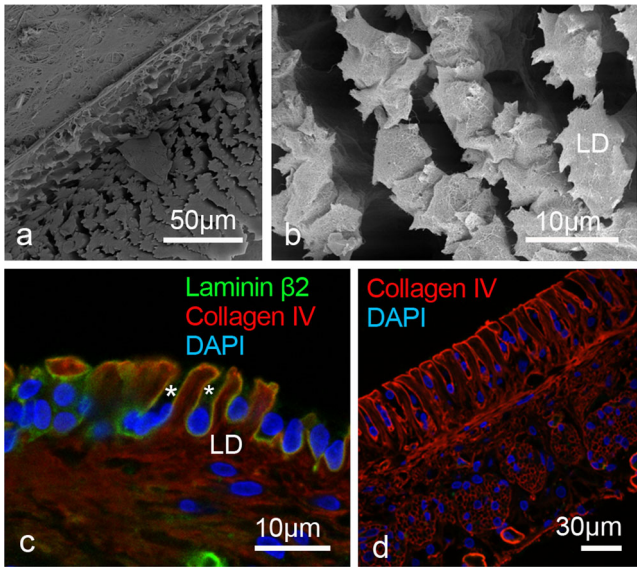


**Fig. 12** SEM and immunohistochemistry of the human spiral limbus. **a**, **b** SEM of cochlea shows limbal dental teeth (*LD*). 54-year-old female. **c** The immunofluoresence of the interdental cells is surrounded by a continuous basement membrane co-expressing laminin-β2 and collagen IV (*asterisks*). 51-year-old male. **d** Confocal immunohistochemistry of collagen IV-labeled basement membranes surrounding the interdental cells, neurons and blood vessels

The LZ of the TM adhered to the surface of the spiral limbus. However, between the LZ and the IDCs was an electron-dense layer (Figs. 13, 14). TEM showed exocytosing vesicles and pits containing floccular material seemingly emerging into the extracellular matrix (Figs. 13, 14c). The secretory-like material seemed to correspond to that observed on the epithelium with SEM (Fig. 4b, c).

## Discussion

TEM studies have shown that the TM consists of both radially oriented type-A fibrils and more or less longitudinally running type-B fibers (Kronester-Frei 1978). Collagen fibrils are embedded in non-collagen matrices composed of several types of glycoproteins (Lukashkin et al. 2012). In the mouse TM, the thick radial collagen bundles are composed of 20-nm thick collagen II fibers embedded in a tectorin-based striated-sheet matrix (Hasko and Richardson 1988; Richardson et al. 2008). For the first time, we analyzed the fine structure of the human TM in tissues immediately fixed at surgery. Findings support those in animals that the TM undergoes continuous changes from base to apex. The width and thickness of the parts (MaZ and MZ) not attached to the spiral limbus tripled while the fibril density, and the diameter of the radial fiber bundles decreased successively from base to apex. Furthermore, the marginal band underwent striking changes with the marginal net containing fine struts in the upper half of the cochlea. These struts showed stereociliary imprints interacting with the fourth row of OHC

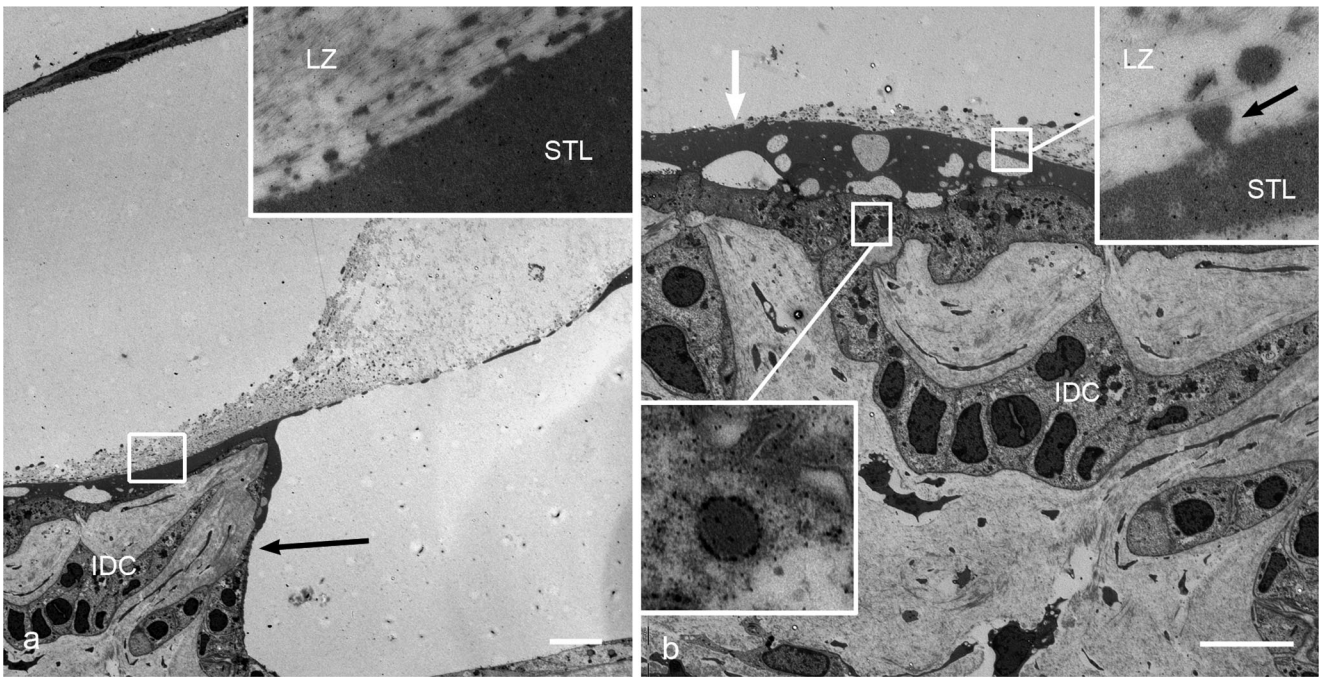


**Fig. 13** TEM of the limbal zone and subtectorial layer of the human tectorial membrane. **a** Between the limbal zone (LZ) and the interdental cells (IDC) is a layer of high electron density. Electron-dense material also appears on the inner sulcus cells (*arrow*). 52-year-old female. **b** TEM of the magnified area in (**a**). The *white arrow* shows the medial termination of the LZ on the electron-dense material. The *inset* in (**a**) and *right inset* (**b**) enlargement of the *framed area* shows that vesicle-like structures (*black arrow*) containing electron-dense material emerge into the TM. The *left inset* in (**b**) shows a dilated endoplasmic reticulum in the IDC. *STL* subtectorial layer. Fixation was conducted in oxygenated fluorocarbon with 2 % glutaraldehyde. Obtained from a 41-year-old female with normal audiometry. *Scale bar* 10 μm

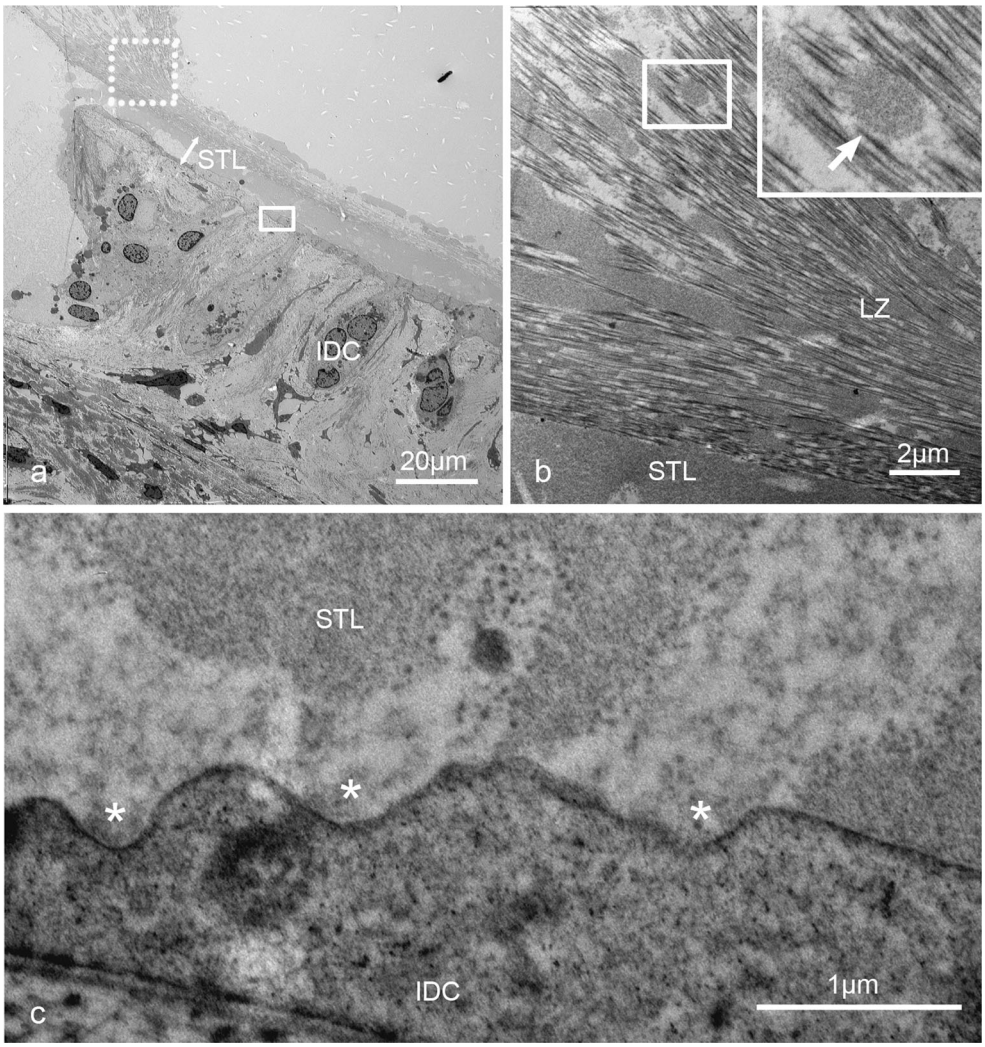


**Fig. 14** TEM of the limbal zone and interdental cells. **a** A low power TEM of the limbal zone resting on the electron-dense layer. The contents of this layer were found to express at least α-tectorin. 54-year-old female. *STL* subtectorial layer, *IDC* interdental cell. The dashed-framed and solid-framed regions are magnified in (**b** and **c**), respectively. **b** The amorphous material (*arrow*) in LZ appears in close association with collagen fibers, as highlighted in the *inset*. **c** The material appears to be secreted from the IDCs to the STL. Several secretory-like pits can be observed (*asterisks*)

hair bundles. Collagen II was strongly expressed with a variable meshwork of an amorphous substance expressing α-tectorin. The collagen fibers were oriented radial, running from the LZ to the marginal band including Kimura's membrane and Hensen's stripe (Hardesty 1915). They formed bundles of various diameters with higher density in the LZ. In the MZ, the radial fiber bundles were thicker in the basal than in the middle turn, which were thicker than in the upper turn. Similarly, the fibers were less densely packed apically in a gradient manner. This may influence TM stiffness in coherence with earlier experiments in the gerbil and mouse hemi-cochlea showing that TM stiffness decreases longitudinally from the base to the apex (Richter et al. 2007; Teudt and Richter 2014).

The α-tectorin expression was found to be stronger in the high-frequency region and in the outer circumference of the TM. This coincided with TEM findings. This could explain why TECTA mutation (4857G→C/exon 14) in the DFNA8/12-affected family causes more hearing loss in humans at high frequencies (Pfister et al. 2004). We did not detect β-tectorin, a protein believed to shape the Hensen's stripe and marginal net. Three human cochleae were stained and the results were not consistent.

Lectin studies of the ear (Gil-Loyzaga et al. 1985; Khalkhali-Ellis et al. 1987; Lim and Rueda 1990) demonstrated that TM polypeptides bind wheat germ and soybean agglutinins, suggesting that they contain *N*-acetyl glucosamine and *N*-acetyl galactosamine (Richardson et al. 1987). Santi et al. (1990) performed electron microscopy of these glycoconjugates of the TM. We established that glycoprotein components are present in the cover net, marginal band, Hansen's stripe and, especially, the LZ, as shown by using fluorescently labeled lectins. A 120-kDa inner ear-specific protein bearing glycosyl groups, otoancorin, was shown to be expressed on the surface of the spiral limbus and believed to be indispensable for the TM to attach to the surface of the spiral limbus (Zwaenepoel et al. 2002; Lukashkin et al. 2012). The gene OTOA encoding this protein was found to be mutated in nonsyndromic recessive deafness DFNB22.

It was surprising to find evidence that the human TM may be replenished and undergo turnover. Several authors have

speculated about possible renewal of TM, and IDCs have been thought to play a crucial role in secreting components into the TM (Iurato 1960; Ishiyama et al. 1970). However, the cellular road and secretory trail have remained tentative (Prieto et al. 1990; Voldrich 1967; Lim 1969, 1972; Thorn et al. 1979). In adult animals, the IDCs have been shown to be secretory and the TM was reported to be produced by the IDCs (Prieto et al. 1990) and supporting cells in the organ of Corti (Lim and Rueda 1990). We noticed that the LZ did not face the IDCs but instead an amorphous layer expressing α-tectorin. It was interposed between the TM and IDCs. TEM performed in mice showed no similar layer (our observations). In the fluorocarbon-fixed human specimen, electron-dense, membrane-bound vesicles appeared in the IDCs. Frequently, endoplasmic sac dilations contained secretory-like protein aggregations. This material seemed to be expelled into the subtectorial layer, even reaching the inner sulcus. The LZ did not face the amorphous layer near Reissner's membrane. Confocal microscopy suggested that α-tectorin was synthesized and secreted from the IDCs into the subtectorial layer of the LZ prior to its incorporation in the LZ (Fig. 15). The TM border, including the marginal band and Kimura's membrane, expressed α-tectorin. The distribution in the MZ and TEM analysis suggested a translocation closely associated with the radial collagen fiber system.

There was various morphology of the marginal band in different parts of the cochlea. In the base, the marginal band was solid and robust suggesting a larger mass load. In the middle turn, the marginal band was delicate and displayed a marginal network, which in earlier literature was based on animal work, and named "randfasernetz". In human TEM sections, a marginal net with fine struts was attached to the Deiters pillar heads adjacent to Hensen's cells that appeared to keep the TM close to the reticular lamina (Glueckert et al. 2005). It is thought to anchor the TM onto the lateral aspect of the acoustic ridge. We found that these struts were an integral part of the acoustic receptor because they displayed stereocilia imprints on the subsurface from the outermost OHCs. The distribution of stereocilia from the OHCs mirrored the architecture of the struts suggesting a reciprocal interaction.

A system of radial fiber bundles running in the bottom of the TM between Hensen's stripe and the marginal band was observed. These fibers were intimately related to the glycoprotein matrix of the OHC imprints and Hensen's stripe. One may assume that these strings could constitute a functional link between the receptor cells. A radial coupling might synchronize equally tuned OHCs to enhance sensitivity and frequency resolution (Gavara and Chadwick 2009). Similarly, radial fibers could even couple the two hair cell systems. However, the absence of stereociliary imprints from IHCs in most species, including human, indicates that IHC hair bundles are freestanding, although one cannot deny the possibility that they could touch the TM during basilar membrane motion (Lim 1986). Our SEM studies of the human TM showed no surface imprints on Hensen's stripe, in accordance with earlier reports (Kimura 1966; Kawabata and Nomura 1981). In another study (Hoshino 1981), SEM of human cochleae showed imprints of IHC stereocilia in the basal turn but not in the apical and middle turns. Based on our findings, we speculate that the radial fiber bundles facing the subtectorial space may contribute to the stiffness in the inferior surface of the TM enabling it to maintain a certain distance from the reticular lamina.

In conclusion, the present study shows the various anatomy of the human TM from base to apex, including collagen fibril organization and distribution of the macromolecular matrix system. In addition, this extracellular matrix seems to be replenished.

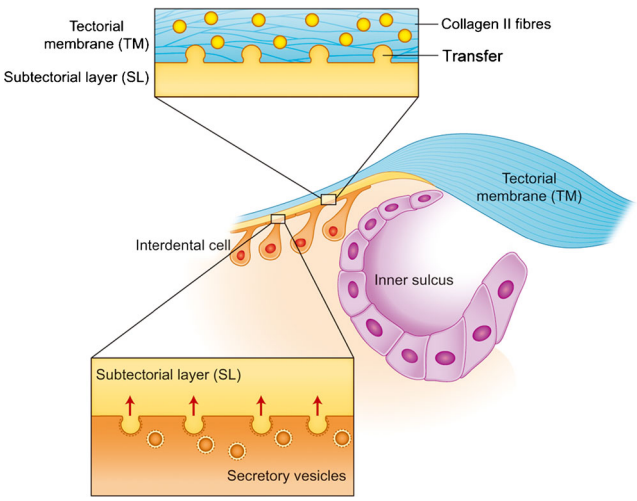


**Fig. 15** Graphic illustration of proposed secretory pathway and uptake of macromolecular substances into the human tectorial membrane. Secretory-like vesicles appear in the apical cytoplasm of the interdental cells (*lower box*). Their contents empty into the subtectorial space forming a subtectorial layer (*STL*) of macromolecular substances. Furthermore, the macromolecular substance is incorporated into the limbal zone of the tectorial membrane in close association with the collagen II fibers (*upper box*)

**Acknowledgments** This study was supported by ALF grants from Uppsala University Hospital and Uppsala University and by the Tysta Skolan Foundation, Swedish Deafness Foundation (HRF) and Land Tirol Technologie Förderungsprogram, Förderung von Wissenschaft, Forschung und Entwicklung (Programm K-Regio Vamel) and Med El, Innsbruck, Austria. Our research is part of the European Community 7th Framework Programme on Research, Technological Development and Demonstration. Project acronym: NANOCI. Grant agreement no: 281056. It was also supported by kindly donated private funds from Börje Runögård, Sweden. Dr. Klaus Qvortrup is acknowledged for providing oxygenated fluorocarbon fixative for the TEM investigation.

## References


Alasti F, Sanati MH, Behrouzifard AH, Sadeghi A, de Brouwer AP, Kremer H, Smith RJ, Van Camp G (2008) A novel TECTA mutation confirms the recognizable phenotype among autosomal recessive hearing impairment families. Int J Pediatr Otorhinolaryngol 72: 249–55

Gavara N, Chadwick RS (2009) Collagen-based mechanical anisotropy of the tectorial membrane: implications for inter-row coupling of outer hair cell bundles. PLoS ONE 4:e4877

Ghaffari R, Aranyosi AJ, Freeman DM (2007) Longitudinally propagating traveling waves of the mammalian tectorial membrane. Proc Natl Acad Sci U S A 104:16510–16515

Gil-Loyzaga P, Raymond J, Gabrion J (1985) Carbohydrates detected by lectins in the vestibular organ. Hear Res 18:269–272

Glueckert R, Pfaller K, Kinnefors A, Schrott-Fischer A, Rask-Andersen H (2005) High resolution scanning electron microscopy of the human organ of Corti. A study using freshly fixed surgical specimens. Hear Res 199:40–56

Hardesty I (1915) On the proportions, development and attachment of the tectorial membrane. Am J Anat 18:1–73

Hasko JA, Richardson GP (1988) The ultrastructural organization and properties of the mouse tectorial membrane matrix. Hear Res 35:21–38

Hilding AC (1952) Studies on the otic labyrinth. On the origin and insertion of the tectorial membrane. Ann Otol Rhinol Laryngol 61:354–70

Hoshino T (1981) Imprints of the inner sensory cell hairs on the human tectorial membrane. Arch Otorhinolaryngol 232:65–71

Hoshino T (1977) Contact between the tectorial membrane and the cochlear sensory hairs in the human and the monkey. Arch Otorhinolaryngol 217:53–60

Hubbard A (1993) A traveling-wave amplifier model of the cochlea. Science 259:68–71

Iurato S (1960) Submicroscopic structure of the membranous labyrinth. 1. The tectorial membrane. Z Zellforsch Mikrosk Anat 52:105–28

Ishiyama E, Weibel J, Keels EW, Richardson TL (1970) Ultrastructure of the interdental cells in mammals. Pract Otorhinolaryngol (Basel) 32:321–34

Khalkhali-Ellis Z, Hemming FW, Steel KP (1987) Glycoconjugates of the tectorial membrane. Hear Res 25:185–191

Kawabata I, Nomura Y (1981) The imprints of the human tectorial membrane. Acta Otolaryngol 91:29–35

Kimura RS (1966) Hairs of the cochlear sensory cells and their attachment to the tectorial membrane. Acta Otolaryngol 61:55–72

Kronester-Frei A (1978) Ultrastructure of the different zones of the tectorial membrane. Cell Tissue Res 193:11–23

Legan PK, Lukashkina VA, Goodyear RJ, Kössi M, Russell IJ, Richardson GP (2000) A targeted deletion in alpha-tectorin reveals that the tectorial membrane is required for the gainand timing of cochlear feedback. Neuron 28:273–285

Lim DJ (1969) Three dimensional observation of the inner ear with the scanning electron microscope. Acta Otolaryngol Suppl 255:1–38

Lim DJ (1972) Fine morphology of the tectorial membrane. Its relationship to the organ of Corti. Arch Otolaryngol 96:199–215

Lim DJ (1986) Functional structure of the organ of Corti: a review. Hear Res 22:117–146

Lim DJ, Rueda J (1990) Distribution of glycoconjugates during cochlea development. A histochemical study. Acta Otolaryngol 110:224–233

Liu W, Boström M, Kinnefors A, Rask-Andersen H (2009) Unique expression of connexins in the human cochlea. Hear Res 250:55–62

Lukashkin AN, Lukashkina VA, Legan PK, Richardson GP, Russell IJ (2004) Role of the tectorial membrane revealed by otoacoustic emissions recorded from wild-type and transgenic Tecta(deltaENT/deltaENT) mice. J Neurophysiol 91:163–71

Lukashkin AN, Legan PK, Weddell TD, Lukashkina VA, Goodyear RJ, Welstead LJ, Petit C, Russell IJ, Richardson GP (2012) Mouse model for human deafness DFNB22 reveals that hearing impairment is due to a loss of inner hair cell stimulation. Proc Natl Acad Sci U S A 109:19351–19356

Meaud J, Grosh K (2010) The effect of tectorial membrane and basilar membrane longitudinal coupling in cochlear mechanics. J Acoust Soc Am 127:1411–1421

Mustapha M, Weil D, Chardenoux S, Elias S, El-Zir E, Beckmann JS, Loiselet J, Petit C (1999) An alpha-tectorin gene defect causes a newly identified autosomal recessive form of sensorineural pre-lingual non-syndromic deafness, DFNB21. Hum Mol Genet 8:409–412

Møller MN, Caye-Thomasen P, Qvortrup K (2013) Oxygenated fixation demonstrates novel and improved ultrastructural features of the human endolymphatic sac. Laryngoscope 123:1967–1975

Pfister M, Thiele H, Van Camp G, Fransen E, Apaydin F, Aydin O, Leistenschneider P, Devoto M, Zenner HP, Blin N, Nürnberg P, Ozkarakas H, Kupka S (2004) A genotype-phenotype correlation with gender-effect for hearing impairment caused by TECTA mutations. Cell Physiol Biochem 14:369–376

Prieto JJ, Rueda J, Merchan JA (1990) Two different secretion mechanisms in the inner ear's interdental cells. Hear Res 45:51–61

Rask-Andersen H, Liu W, Erixon E, Kinnefors A, Pfaller K, Schrott-Fischer A, Glueckert R (2012) Human cochlea: anatomical characteristics and their relevance for cochlear implantation. Anat Rec (Hoboken) 295:1791–1811

Richardson GP, Russell IJ, Duance VC, Bailey AJ (1987) Polypeptide composition of the mammalian tectorial membrane. Hear Res 25:45–60

Richardson GP, Lukashkin AN, Russell IJ (2008) The tectorial membrane: one slice of a complex cochlear sandwich. Curr Opin Otolaryngol Head Neck Surg 16:458–464

Richter CP, Emadi G, Getnick G, Quesnel A, Dallos P (2007) Tectorial membrane stiffness gradients. Biophys J 93:2265–2276

Rubio ME, Rueda J, Prieto JJ, Merchán JA (1994) Pilocarpine-induced changes in the saccharide composition of the tectorial membrane and interdental cells of the organ of Corti: a study with gold-labeled lectins. J Histochem Cytochem 42:405–16

Russell IJ, Legan PK, Lukashkina VA, Lukashkin AN, Goodyear RJ, Richardson GP (2007) Sharpened cochlear tuning in a mouse with a genetically modified tectorial membrane. Nat Neurosci 10:215–23

Santi PA, Lease MK, Harrison RG, Wicker EM (1990) Ultrastructure of proteoglycans in the tectorial membrane. J Electron Microsc Tech 15:293–300

Sellon JB, Ghaffari R, Farrahi S, Richardson GP, Freeman DM (2014) Porosity controls spread of excitation in tectorial membrane traveling waves. Biophys J 106:1406–1413

Simmler MC, Cohen-Salmon M, El-Amraoui A, Guillaud L, Benichou JC, Petit C, Panthier JJ (2000) Targeted disruption of otog results in deafness and severe imbalance. Nat Genet 24:139–143

Spoendlin H, Schrott A (1988) The spiral ganglion and the innervation of the human organ of Corti. Acta Otolaryngol 105:403–410

Steel KP (1983) The tectorial membrane of mammals. Hear Res 9:327–359

Tanaka K, Smith CA (1975) Structure of the avian tectorial membrane. Ann Otol Rhinol Laryngol 84:287–296

Teudt IU, Richter CP (2014) Basilar Membrane and Tectorial Membrane Stiffness in the CBA/CaJ Mouse. J Assoc Res Otolaryngol 15:675–694

Thorn L, Arnold W, Schinko I, Wetzstein R (1979) The limbus spiralis and its relationship to the developing tectorial membrane in the cochlear duct of the Guinea pig fetus. Anat Embryol (Berl) 155: 303–310

Tylstedt S, Kinnefors A, Rask-Andersen H (1997) Neural interaction in the human spiral ganglion: a TEM study. Acta Otolaryngol 117:505–512

Voldrich L (1967) Morphology and function of the epithelium of the limbus spiralis cochleae. Acta Otolaryngol 63:503–514

Verhoeven K, Van Laer L, Kirschhofer K, Legan PK, Hughes DC, Schatteman I, Verstreken M, Van Hauwe P, Coucke P, Chen A, Smith RJ, Somers T, Offeciers FE, Van de Heyning P, Richardson GP, Wachtler F, Kimberling WJ, Willems PJ, Govaerts PJ, Van Camp G (1998) Mutations in the human alpha-tectorin gene cause autosomal dominant non-syndromic hearing impairment. Nat Genet 19:60–62

Verpy E, Masmoudi S, Zwaenepoel I, Leibovici M, Hutchin TP, Del Castillo I, Nouaille S, Blanchard S, Laine S, Popot JL, Moreno F, Mueller RF, Petit C (2001) Mutations in a new gene encoding a protein of the hair bundle cause non-syndromic deafness at the DFNB16 locus. Nat Genet 29:345–349

Zheng J, Miller KK, Yang T, Hildebrand MS, Shearer AE, DeLuca AP, Scheetz TE, Drummond J, Scherer SE, Legan PK, Goodyear RJ, Richardson GP, Cheatham MA, Smith RJ, Dallos P (2011) Carcinoembryonic antigen-related cell adhesion molecule 16 interacts with alpha-tectorin and is mutated in autosomal dominant hearing loss (DFNA4). Proc Natl Acad Sci U S A 108:4218–4223

Zwaenepoel I, Mustapha M, Leibovici M, Verpy E, Goodyear R, Liu XZ, Nouaille S, Nance WE, Kanaan M, Avraham KB, Tekaia F, Loiselet J, Lathrop M, Richardson G, Petit C (2002) Otoancorin, an inner ear protein restricted to the interface between the apical surface of sensory epithelia and their overlying acellular gels, is defective in autosomal recessive deafness DFNB22. Proc Natl Acad Sci U S A 99: 6240–6245